Quasi-geostrophic dynamics of a finite-depth tropopause

R. Plougonven[*] and J. Vanneste[†]

[*]Laboratoire de Météorologie Dynamique du CNRS
Ecole Normale Supérieure, IPSL, 24, rue Lhomond, 75231 Paris cedex 05, France

[†]School of Mathematics and Maxwell Institute for Mathematical Sciences
University of Edinburgh, Edinburgh EH9 3JZ, UK

March 2010

Abstract

A model of tropopause dynamics is derived which is of intermediate complexity between the three-dimensional quasi-geostrophic model and the surface quasi-geostrophic (SQG) model. The model assumes that a sharp transition in stratification occurs over a small but finite tropopause region separating regions of uniform potential vorticity. The model is derived using a matched-asymptotics technique, with the ratio of the depth of the tropopause region to the typical vertical scale of perturbations outside as small parameter. It reduces to SQG to leading-order in this parameter, but takes into account the next-order correction. As a result it remains three-dimensional, although with a potential-vorticity inversion relation that is greatly simplified compared to the Laplacian inversion of quasi-geostrophic theory.

The model is applied to examine the linear dynamics of perturbations at the tropopause. Edge waves, described in the SQG approximation, are recovered, and explicit expressions are obtained for the corrections to their frequency and structure that result from the finiteness of the tropopause region. The sensitivity of these corrections to the stratification and shear profiles across the tropopause is investigated. In addition, the evolution of perturbations with near zero vertically integrated potential vorticity is discussed. These perturbations, which are filtered out by the SQG approximation, are represented by a continuous spectrum of singular modes and evolve as sheared disturbances. The decomposition of arbitrary perturbations into edge wave and continuous-spectrum contributions is discussed.

1 Introduction

Tropopause motion plays a crucial part in the dynamics of the atmosphere. Important features of the tropospheric and lower-stratospheric circulation at mid-latitude can indeed be well described by considering only balanced motion at the tropopause, near the ground and their interactions (Hoskins et al. 1985). Furthermore, the role of the tropopause as a barrier to transport makes it crucial for the distribution of atmospheric tracers such as water vapour or ozone. The simplest model of the tropopause treats it in the quasi-geostrophic approximation as a rigid lid above a uniform potential-vorticity (PV) environment. The dynamics is then entirely controlled by the potential-temperature anomaly at the tropopause which is materially conserved. This model, also suitable to describe the dynamics of low-level potential-temperature anomalies, is the surface quasi-geostrophic (SQG) model (Blumen 1978, Pierrehumbert et al. 1994, Held et al. 1995) which has attracted renewed attention in recent year in the atmospheric (e.g. Tulloch & Smith 2006), oceanographic (e.g. Lapeyre & Klein 2006) and mathematical (e.g. Kiselev et al. 2007) communities.

The rigid-lid assumption was relaxed by Juckes (1994) who replaced it by the more realistic assumption of a finite jump in the stratification at the tropopause (see also Rivest et al. 1992, Rivest & Farrell 1992). The resulting model remains the SQG model, with a relationship between potential-temperature and velocity that involves the Brunt-Väisälä frequency N both of the troposphere and of the stratosphere. Among other things, this makes it possible to relate the potential-temperature anomalies to vertical displacements of the tropopause.

SQG provides a useful first model of tropopause dynamics. The approximations on which it relies, namely quasi-geostrophic dynamics and a sharp jump in N separating two regions with uniform PV, are of course idealisations, and it is of interest to examine the effect of relaxing them. Weak non-zero interior PV gradients were introduced by Rivest et al. (1992) and Rivest & Farrell (1992) in a linearised model. They showed how the edge (or Eady) waves which propagate along the tropopause in the SQG model become weakly damped Landau modes (or quasi modes) as a result of the formation of a critical layer (see Briggs et al. 1970, Balmforth et al. 2001, for analogous effects in two-dimensional fluids). On the other hand, Muraki & Hakim (2001) and Hakim et al. (2002) carried out the Rossby-number expansion underlying the quasi-geostrophic model to one order higher in order to examine the asymmetries between cyclones and anti-cyclones induced by balanced ageostrophic terms. In the present paper, we relax the third key assumption of the SQG model of the tropopause, the assumption of a discontinuity in N.

Specifically, to assess the role played by the internal structure of the tropopause, we replace the (infinitely sharp) vertical jump in N by a smooth transition. Although smooth, this transition is assumed to take place over a vertical scale that is small compared to the typical vertical scales of the motion (given by f/N times the horizontal scales, where f is the Coriolis parameter). This assumption makes it possible to apply a matched-asymptotic technique and obtain a reduced model describing the dynamics of a PV anomaly localised in the tropopause region. To leading order in the small parameter ϵ characterising the vertical-scale separation, this model reduces to the SQG model, with a dynamics controlled by the vertically integrated PV anomaly, which can be interpreted as a potential temperature. At the next order, however, the vertical structure of the PV anomaly needs to be taken into account. This evolves as a result of (i) advection by the basic shear flow which is present across the tropopause region, and (ii) advection of the basic PV profile (associated with the basic shear-flow and Brunt–Väisälä frequency profiles) by the altitude-dependent velocity perturbation. Although the model obtained remains three-dimensional, it is a reduction of the original three-dimensional quasi-geostrophic equations in that it concentrates on

the shallow tropopause region, removing the need for solving for the various fields outside that region. Like similar models in the theory of critical layers (e.g. Stewartson 1981) or PV defects (Balmforth et al. 1997, Samelson 1999) it also involves a simplified inversion relation between the PV and velocity fields which results from the strong anisotropy of the flow.

We confine our applications of the reduced model to its linear dynamics. In the SQG description, this is limited to the propagation of edge waves. These are recovered here: the frequency of the SQG approximation, which is obtained to leading order in ϵ, is corrected at the next order. We find an explicit expression for this correction which depends on the stratification and shear profiles within the tropopause region. We also provide details about the vertical structure of the edge waves.

Because our model can represent the vertical structure of the PV perturbation, its dynamics is much richer than that of the SQG model. At the linear level, this results in the existence of a continous spectrum of singular modes which represents sheared disturbances localised near the tropopause. We examine the dynamics of these disturbances and show how they co-exist with the edge waves.

The plan of the paper is as follows. In section 2, we derive the simplified model for perturbations to a finite-depth tropopause using matched asymptotics. Only the main steps of the derivation are described there, with details relegated to appendices. The linear dynamics of the model is then examined in section 3: the two modes of motion, namely edge waves and continuous-spectrum perturbations, are identified, and the nature of their dynamics is discussed. The main effect of a smooth tropopause on edge waves is to shift their frequency compared to that obtained in the SQG approximation. We analyse the sensitivity of this frequency shift to the stratification and shear profiles across the tropopause in section 4. The paper concludes with a discussion in section 5.

2 Derivation

We start with the three-dimensional quasi-geostrophic equation in the form

$$\partial_t q + \partial(\psi, q) = 0 \quad \text{and} \quad q = \partial_{xx}^2 \psi + \partial_{yy}^2 \psi + \partial_z \left(S \partial_z \psi \right), \tag{2.1}$$

for the PV q and streamfunction ψ. Here $\partial(\psi, q) = \partial_x \psi \partial_y q - \partial_y \psi \partial_x q$, and the parameter S is defined as

$$S = f^2/N^2,$$

where f is the Coriolis parameter and N the Brunt–Väisälä frequency. Note that we have adopted the Boussinesq form of the quasi-geostrophic approximation for simplicity only; it is not difficult, though somewhat cumbersome, to generalise our developments to the compressible version of (2.1).

The tropopause is characterised by an abrupt change in N, from its tropospheric value N_- to its stratospheric value N_+ as z goes through 0, the altitude we choose for the undisturbed tropopause. To make this explicit, we introduce the small parameter $\epsilon \ll 1$ and the stretched vertical coordinate

$$Z = \epsilon^{-1} z,$$

and write

$$S = S(Z).$$

The function S is monotonically decreasing, with $O(1)$ variations and

$$\lim_{Z \to \pm\infty} S(Z) = S_\pm = f^2/N_\pm^2.$$

3

We take into account the presence of a large-scale zonal shear flow, with streamfunction $\Psi = -yU(z)$. Motivated by observations, this flow is assumed linear in z outside the tropopause region; this is made explicit by writing

$$U(z) = \epsilon \int_0^{z/\epsilon} \Sigma(Z')\, dZ' = \epsilon v(Z).$$

where the shear Σ is assumed to approach constant values for $|Z| \to \infty$:

$$\lim_{Z \to \pm\infty} \Sigma(Z) = \Sigma_\pm,$$

so that the velocity satisfies $U(z) \sim \Sigma_\pm z$ as $z \to \pm\infty$. The PV associated with this basic flow is given by

$$Q = -y\frac{\mathrm{d}}{\mathrm{d}z}(S\Sigma) = -\epsilon^{-1}y\sigma', \tag{2.2}$$

where the prime denotes differentiation with respect to Z. Here, we have introduced

$$\sigma(Z) = S(Z)\Sigma(Z).$$

Like S and Σ, this function is bi-asymptotic to constants:

$$\lim_{Z \to \pm\infty} \sigma = \sigma_\pm = S_\pm\Sigma_\pm.$$

Its derivative, $\sigma' = O(1)$, is the negative of the scaled meridional gradient of PV.

We examine the dynamics of small-amplitude perturbations to the basic flow. Introducing the decomposition $\psi = \Psi + \epsilon\psi'$ and $q = Q + \epsilon q'$ into (2.1) and dropping the primes leads to

$$\partial_t q + \epsilon v \partial_x q - \epsilon^{-1}\sigma' \partial_x \psi + \epsilon \partial(\psi, q) = 0 \quad \text{and} \quad q = \partial_{xx}^2 \psi + \partial_{yy}^2 \psi + \partial_z\left(S\partial_z\psi\right). \tag{2.3}$$

Note that we have chosen to scale the perturbation amplitudes by the small parameter ϵ characterising the depth of the tropopause. This is motivated by a standard dominant-balance argument: with this scaling, the effects of the nonlinear terms in (2.3) and those associated with the finite tropopause depth have the same order of magnitude.

The system (2.3) can be simplified for $\epsilon \ll 1$ using matched asymptotics. In two outer regions, where $|z| \gg \epsilon$, we can take $q = 0$ (since $S' = 0$). The perturbation streamfunction ψ then satisfies a scaled Laplace equation, where the derivatives with respect to z are scaled by $S_\pm^{1/2}$. This equation is solved by introducing the horizontal Fourier transform $\hat{\psi}(k, l, z, t)$, with

$$\psi(x, y, z, t) = \int_{-\infty}^{\infty} \int_{-\infty}^{\infty} \mathrm{e}^{\mathrm{i}(kx+ly)}\hat{\psi}(k, l, z, t)\, \mathrm{d}k\mathrm{d}l$$

to obtain

$$\hat{\psi}(k, l, z, t) = \hat{\phi}_\pm(k, l, t)\mathrm{e}^{\mp\kappa z/S_\pm^{1/2}}, \tag{2.4}$$

where $\kappa > 0$ is defined by

$$\kappa^2 = k^2 + l^2,$$

and the upper (lower) sign refers to $z > 0$ ($z < 0$). The as yet unkown functions $\hat{\phi}_\pm(k, l, t)$ can now be expanded in power series according to

$$\hat{\phi}_\pm(k, l, t) = \hat{\phi}_\pm^{(0)}(k, l, t) + \epsilon\hat{\phi}_\pm^{(1)}(k, l, t) + \cdots. \tag{2.5}$$

4

The functions $\hat{\phi}_{\pm}^{(k)}$, $k = 0, 1, \cdots$ are determined next by examining the relationship between ψ and q in the tropopause region $z = O(\epsilon)$, that is $Z = O(1)$.

In this inner region, we use Z as vertical coordinate, expand the streamfunction as

$$\psi(x, y, z, t) = \psi^{(0)}(x, y, t) + \epsilon \psi^{(1)}(x, y, Z, t) + \cdots \tag{2.6}$$

and leave the PV q unexpanded. In writing (2.6), we have anticipated that the leading-order streamfunction is independent of Z.

In what follows we determine the first two terms in the expansion of ψ and therefore approximate the dynamics up to errors of order $O(\epsilon^2)$. The relationship between the outer and inner expansions (2.4) and (2.6) follows from matching conditions. Expanding (2.4) for small Z and comparing with (2.6) first gives the matching condition

$$\hat{\psi}^{(0)}(k, l, t) = \hat{\phi}_{\pm}^{(0)}(k, l, t), \tag{2.7}$$

which shows that the leading-order streamfunction is continuous across the tropopause. At the next two orders we find

$$\hat{\psi}^{(1)}(k, l, Z, t) \sim \mp \frac{\kappa}{S_{\pm}^{1/2}} \hat{\phi}_{\pm}^{(0)}(k, l, t) Z + \hat{\phi}_{\pm}^{(1)}(k, l, t) \tag{2.8}$$

$$\hat{\psi}^{(2)}(k, l, Z, t) \sim \frac{\kappa^2}{S_{\pm}} \hat{\phi}_{\pm}^{(0)}(k, l, t) \frac{Z^2}{2} \mp \frac{\kappa}{S_{\pm}^{1/2}} \hat{\phi}_{\pm}^{(1)}(k, l, t) Z + \hat{\phi}_{\pm}^{(2)}(k, l, t), \tag{2.9}$$

as $Z \to \pm\infty$. The PV–streamfunction relation takes the form

$$q = \partial_Z \left(S \partial_Z \psi^{(1)} \right) + \epsilon \left[\partial_{xx}^2 \psi^{(0)} + \partial_{yy}^2 \psi^{(0)} + \partial_Z \left(S \partial_Z \psi_2 \right) \right] + \cdots,$$

giving

$$\partial_Z \left(S \partial_Z \psi^{(1)} \right) = q \tag{2.10}$$

$$\text{and} \quad \partial_{xx}^2 \psi^{(0)} + \partial_{yy}^2 \psi^{(0)} + \partial_Z \left(S \partial_Z \psi^{(2)} \right) = 0. \tag{2.11}$$

Combining these two equations with the matching conditions (2.7)–(2.9), it is possible to relate explicity $\psi^{(0)}$ and $\psi^{(1)}$ to q. Computations detailed in Appendix A lead to

$$\hat{\psi}^{(0)}(k, l, t) = -\frac{\hat{\theta}(k, l, t)}{\kappa(S_+^{1/2} + S_-^{1/2})}, \quad \text{where} \quad \hat{\theta}(k, l, t) = \int_{-\infty}^{\infty} \hat{q}(k, l, Z, t) \, \mathrm{d}Z, \tag{2.12}$$

and

$$\begin{aligned}
\hat{\psi}^{(1)}(k, l, Z, t) &= \frac{S_+^{1/2}}{S_+^{1/2} + S_-^{1/2}} \int_Z^{\infty} \frac{\mathrm{d}Z'}{S(Z')} \int_{Z'}^{\infty} \hat{q}(k, l, Z'', t) \, \mathrm{d}Z'' \\
&+ \frac{S_-^{1/2}}{S_+^{1/2} + S_-^{1/2}} \int_{-\infty}^{Z} \frac{\mathrm{d}Z'}{S(Z')} \int_{-\infty}^{Z'} \hat{q}(k, l, Z'', t) \, \mathrm{d}Z'' \\
&- \frac{\hat{\theta}}{\left(S_+^{1/2} + S_-^{1/2} \right)^2} \left(\int_Z^{\infty} \left(\frac{S_+}{S(Z')} - 1 \right) \mathrm{d}Z' + \int_{-\infty}^{Z} \left(\frac{S_-}{S(Z')} - 1 \right) \mathrm{d}Z' \right).
\end{aligned} \tag{2.13}$$

5

These two equations complement the PV equation (2.3) which, in the tropopause region, reduces to

$$\partial_t q + \epsilon \upsilon \partial_x q - \sigma' \partial_x (\psi^{(0)} + \epsilon \psi^{(1)}) + \epsilon \partial(\psi^{(0)}, q) = 0, \qquad (2.14)$$

after neglecting $O(\epsilon^2)$ terms. The closed dynamical system (2.12)–(2.14) is the first result of this paper. It provides a simplified model for the quasi-geostrophic dynamics of the tropopause region that takes into account the fact that the transition in N takes place over a finite depth. It does so by including $O(\epsilon)$ terms that are neglected in the standard derivation leading to the SQG model. This model is recovered formally by the rescaling $(\psi, q) \mapsto \epsilon^{-1}(\psi, q)$ followed by setting $\epsilon = 0$. The remaining terms in (2.14) can then be integrated with respect to Z to obtain the two-dimensional system

$$\partial_t \theta - (\sigma_+ - \sigma_-)\partial_x \psi^{(0)} + \partial(\psi^{(0)}, \theta) = 0, \qquad (2.15)$$

closed by (2.12). This can be recognised as the SQG model (Juckes 1994) in the presence of a background meridional gradient of potential temperature. Note that with the definition given in (2.12), θ is better interpreted as the depth-integrated PV rather than a potential temperature. The tropopause potential temperature as defined by Juckes (1994) corresponds to θ up to a constant dimensional factor.

Another model that can be recovered from (2.12)–(2.14) is the defect model of Samelson (1999). This arises when the variations in N^2 and hence in S are $O(\epsilon)$. In that case, $\tilde{S}' = S'/\epsilon = O(1)$, and time can be rescaled as $T = \epsilon t$. With the further simplification of constant shear $\Sigma(Z) = \text{const.}$, we obtain

$$\partial_T q + \Sigma Z \partial_x q - \Sigma \tilde{S}' \partial_x \psi^{(0)} + \partial(\psi^{(0)}, q) = 0, \qquad (2.16)$$

closed by (2.12) where S_+ and S_- can be taken as the same value. (The defect model is in fact somewhat more general since the basic PV gradient, here $-\Sigma \tilde{S}'$, can include a contribution from a localised departure of the background shear from its constant value Σ.)

Unlike the SQG model, but like the defect model, the new model (2.12)–(2.14) retains the three dimensions of its parent, the quasi-geostrophic model. Its main advantage is of course that it focuses on the shallow tropopause region, with no need to resolve the far-field region since this has been treated analytically. The PV inversion (2.12)–(2.13) is also explicit and hence substantially simpler than the inversion of the Laplacian operator that appears in the quasi-geostrophic model. Note that the approximation of this operator involves successively higher powers of the horizontal wavenumber κ (with κ^{-1} appearing in $\hat{\psi}^{(0)}$, κ^0 in $\hat{\psi}^{(1)}$, etc.). This indicates, unsurprisingly, that the model is unsuitable to examine horizontal scales that are (ϵ) or smaller; the dynamics of these is essentially isotropic (in the scaled coordinates), and can only be described by the full quasi-geostrophic model.

One of the interests of the model (2.12)–(2.14) is to separate explicitly the various terms contributing to the dynamics within a finite-depth tropopause. The dominant term in (2.14) is the advection of the meridional PV gradient $-\sigma'$ by the leading-order perturbation velocity $\partial_x \psi^{(0)}$. Because this velocity is independent of altitude, this advection leaves the vertical structure of the perturbation PV unchanged; the leading-order dynamics can therefore be reduced to the evolution of the vertically integrated PV — this is the essence of the SQG model. At the next order, however, the vertical structure of the perturbation PV changes because of the shear (term $\epsilon \upsilon \partial_x q$ in (2.14)), and because of the the z-dependence of the horizontal velocity advecting the basic PV (term $-\sigma' \partial_x \psi^{(1)}$). This results in a much richer dynamics than that of the SQG model, as we now demonstrate by considering the linearisation of (2.14).

6

3 Linear dynamics

We examine how the internal structure of the tropopause modifies the linear dynamics of perturbations. We consider perturbations in the form of plane waves, with

$$q(x, y, Z, t) = \hat{q}(k, l, Z)e^{i(kx+ly-\omega t)} + \text{c.c.},$$

where ω is the frequency. Note that we abuse notation in using the same hatted variables to denote functions of time as in the previous section, and time-independent amplitudes as here; this should not cause confusion. We expand the PV and frequency in powers of ϵ:

$$\hat{q} = \hat{q}_0 + \epsilon\hat{q}_1 + \cdots \quad \text{and} \quad \omega = \omega_0 + \epsilon\omega_1 + \cdots.$$

The streamfunction is then written as the double expansion

$$\hat{\psi} = \hat{\psi}_0 + \epsilon\hat{\psi}_1 + \cdots = \hat{\psi}_0^{(0)} + \epsilon\left(\hat{\psi}_1^{(0)} + \hat{\psi}_0^{(1)}\right) + \cdots,$$

where the superscripts (0) and (1) refer to the two inversion relations (2.12) and (2.13), respectively, so that $\hat{\psi}_0^{(0)}$ and $\hat{\psi}_1^{(0)}$ are Z-independent, while $\hat{\psi}_0^{(1)}$ depends on Z. Introducing these expansions into the linearisation of (2.14) gives to leading order

$$-i\omega_0\hat{q}_0 - i\sigma'k\hat{\psi}_0^{(0)} = 0 \quad \text{with} \quad \hat{\psi}_0^{(0)} = -\frac{1}{\kappa\left(S_+^{1/2} + S_-^{1/2}\right)}\int_{-\infty}^{\infty}\hat{q}_0\,dZ.$$

This equations admits two possible types of solutions. First, egde waves, with frequency

$$\omega_0 = \frac{(\sigma_+ - \sigma_-)k}{\kappa\left(S_+^{1/2} + S_-^{1/2}\right)}, \tag{3.1}$$

which is negative, corresponding to westward propagation, and vertical structure given by

$$\hat{q}_0 = \sigma', \tag{3.2}$$

up to a constant factor. The second type of solutions have zero frequency to leading order, $\omega_0 = 0$, and a vertical structure that is only constrained by the condition

$$\int_{-\infty}^{\infty}\hat{q}_0\,dZ = 0. \tag{3.3}$$

As will become clear, these solutions correspond to the continous spectrum admitted by (2.14). Note that the leading-order structure of an edge wave (3.2) is precisely that obtained when perturbations displace the basic PV profile (2.2) in the meridional direction; on the other hand, the condition (3.3) which ensures no leading-order projection on the edge wave is satisfied by vertical displacements of the basic PV profile, since these are proportional to σ''. Arbitrary initial PV perturbations project on both the edge wave and the continuous spectrum. To leading order, the decomposition into these two contributions is written

$$\hat{q}_0 = \frac{\sigma'}{\sigma_+ - \sigma_-}\int_{-\infty}^{\infty}\hat{q}_0\,dZ + \tilde{q}_0, \tag{3.4}$$

defining the contribution $\tilde{q}_0$ which clearly satisfies (3.3).

At first order in ϵ, we obtain the equation

$$-\mathrm{i}\omega_0 \hat{q}_1 - \mathrm{i}\omega_1 \hat{q}_0 - \mathrm{i}\sigma' k \left(\hat{\psi}_1^{(0)} + \hat{\psi}_0^{(1)} \right) + \mathrm{i}kv\hat{q}_0 = 0, \qquad (3.5)$$

where

$$\hat{\psi}_1^{(0)} = -\frac{1}{\kappa \left(S_+^{1/2} + S_-^{1/2} \right)} \int_{-\infty}^{\infty} \hat{q}_1 \,\mathrm{d}Z, \qquad (3.6)$$

and $\hat{\psi}_0^{(1)}$ is given in terms of $\hat{q}_0$ as $\hat{\psi}^{(1)}$ in terms of $\hat{q}$ in (2.13). From (3.5) we can extract not only an $O(\epsilon)$ correction to the leading-order edge-wave frequency (3.1) but also a correction to their structure (3.2). These corrections are described in detail for both edge waves and continuous-spectrum perturbations below.

3.1 Edge waves

We now consider the edge-wave solutions satisfying (3.1)–(3.2) in more detail. Introducing these equations into (3.5) and integrating with respect to Z yields

$$-\mathrm{i}\omega_1(\sigma_+ - \sigma_-) - \mathrm{i}k \int_{-\infty}^{\infty} \sigma'(Z)\hat{\psi}_0^{(1)} \,\mathrm{d}Z + \mathrm{i}k \int_{-\infty}^{\infty} \sigma'(Z)v(Z) \,\mathrm{d}Z = 0.$$

This gives the correction ω_1 to the frequency as

$$\omega_1 = \frac{-k}{\sigma_+ - \sigma_-} \int_{-\infty}^{\infty} \left[\sigma'(Z)\hat{\psi}_0^{(1)} - \sigma'(Z)v(Z) \right] \,\mathrm{d}Z. \qquad (3.7)$$

A completely explicit form can be obtained by using (2.13) with $\hat{q} = \hat{q}_0 = \sigma'$ and $\hat{\theta} = \sigma_+ - \sigma_-$ to compute $\hat{\psi}_0^{(1)}$. Manipulations detailed in Appendix B then lead to the relatively compact expression

$$\int_{-\infty}^{\infty} \sigma'(Z)\hat{\psi}_0^{(1)} \mathrm{d}Z = \int_{-\infty}^{\infty} \frac{S(Z)(\sigma_+ - \sigma_-)^2 - \left[S_+^{1/2}(\sigma(Z) - \sigma_-) - S_-^{1/2}(\sigma_+ - \sigma(Z)) \right]^2}{\left(S_+^{1/2} + S_-^{1/2} \right)^2 S(Z)} \mathrm{d}Z \qquad (3.8)$$

for the first term appearing in (3.7). This expression can be further simplified in the particular case of a constant shear $\Sigma = \mathrm{const}$. With $\sigma = S\Sigma$, it reduces to

$$\int_{-\infty}^{\infty} \sigma'(Z)\hat{\psi}_0^{(1)} \mathrm{d}Z = \Sigma^2 \int_{-\infty}^{\infty} \frac{[S_+ - S(Z)][S(Z) - S_-]}{S(Z)} \,\mathrm{d}Z,$$

and the complete frequency correction (3.7) takes the neat form

$$\omega_1 = -\frac{\Sigma k}{S_+ - S_-} \int_{-\infty}^{\infty} \frac{[S_+ - S(Z)][S(Z) - S_-] - ZS(Z)S'(Z)}{S(Z)} \,\mathrm{d}Z. \qquad (3.9)$$

Note that our basic assumption that the basic PV gradient vanishes rapidly outside the tropopause region results in purely real frequency corrections. If this vanishing is exponentially fast, in particular, the frequency of the edge wave remains real to all orders in ϵ. By contrast, if a gradient of PV outside the tropopause region is taken into account, the edge waves disappear as strict normal

modes but persist as slowly damped Landau modes or quasi-modes (Rivest et al. 1992, Rivest & Farrell 1992).

With the frequency correction (3.7) determined, the correction to the vertical structure of the edge-wave vorticity follows from (3.5). This correction can be chosen to satisfy

$$\int_{-\infty}^{\infty} \hat{q}_1 \, \mathrm{d}Z = 0, \tag{3.10}$$

which leads to $\hat{\psi}_1^{(0)} = 0$ and hence to the vertical structure

$$\hat{q}_1 = -\frac{\sigma'}{\omega_0} \left(\omega_1 + k\hat{\psi}_0^{(1)} - kv \right), \tag{3.11}$$

where $\psi_0^{(1)}$ is given by the right-hand side of (2.13) with $q = \sigma'$ on the right-hand side. Note that the expression (3.7) for ω_1 ensures consistency with (3.10).

3.2   Continuous spectrum

The perturbations with vertically integrated PV vanishing at leading order, that is, verifying (3.3), satisfy $\omega_0 = 0$. The structure of the next order correction can be obtained by integrating (3.5) with respect to Z, which gives a compatibility condition determining $\hat{\psi}_1^{(0)}$ in terms of $\hat{q}_0$:

$$(\sigma_+ - \sigma_-)\hat{\psi}_1^{(0)} = -\int_{-\infty}^{\infty} \sigma'(Z)\hat{\psi}_0^{(1)}(Z) \, \mathrm{d}Z + \int_{-\infty}^{\infty} v(Z)\hat{q}_0(Z) \, \mathrm{d}Z. \tag{3.12}$$

Noting that from (2.13)

$$\hat{\psi}_0^{(1)} = \frac{S_+^{1/2}}{S_+^{1/2} + S_-^{1/2}} \int_Z^{\infty} \frac{\mathrm{d}Z'}{S(Z')} \int_{Z'}^{\infty} \hat{q}_0(Z'') \, \mathrm{d}Z''$$

$$+ \frac{S_-^{1/2}}{S_+^{1/2} + S_-^{1/2}} \int_{-\infty}^{Z} \frac{\mathrm{d}Z'}{S(Z')} \int_{-\infty}^{Z'} \hat{q}_0(Z'') \, \mathrm{d}Z'',$$

this determines $\hat{\psi}_1^{(0)}$ as expected.

In view of (2.12), condition (3.12) provides the constraint

$$\int_{-\infty}^{\infty} \hat{q}_1 \, \mathrm{d}Z = \frac{(S_+^{1/2} + S_-^{1/2})\kappa}{\sigma_+ - \sigma_-} \left(\int_{-\infty}^{\infty} \sigma'(Z)\hat{\psi}_0^{(1)}(Z) \, \mathrm{d}Z - \int_{-\infty}^{\infty} v(Z)\hat{q}_0(Z) \, \mathrm{d}Z \right) \tag{3.13}$$

on the integrated PV. This shows that, to be dynamically split from edge waves, perturbations need to have not only a zero integrated PV at leading-order, but also a specific vertically integrated PV at the next order. In the same way as (3.10) could be imposed for the structure of edge waves, here any vertical profile satisfying (3.13) can be taken for the structure of these perturbations.

The PV then satisfies

$$(v(Z) - c_1)\hat{q}_0 - \sigma' \left(\hat{\psi}_1^{(0)} + \hat{\psi}_0^{(1)} \right) = 0, \quad \text{where} \quad c_1 = \omega_1/k.$$

Since v ranges from $-\infty$ to ∞ (if $\Sigma_+\Sigma_- > 0$), there is a continuous spectrum of (singular) modes, for $-\infty < c_1 < \infty$. Thus, assuming that there are no eigenvalue embedded in this continuous

spectrum, perturbations that satisfy (3.3) are represented completely by a superposition of singular modes parameterized by c_1. The evolution of such perturbation can be expected to be that typical of sheared disturbances, with a vorticity that is sheared by the basic flow and reduced to small scales for large times.

The full picture of the linear evolution is then relatively simple. Given an initial distribution of PV, a part $\sigma' \int q \, dZ$ evolves as an edge wave, while the remainder, with an associated streamfunction that is $O(\epsilon)$, evolves as a sheared disturbance, with the streamfunction (and energy) decreasing. The energy of the continuous-spectrum perturbations can be expected to behave in the same way as in two-dimensional shear flows, namely decay like t^{-2} since the PV-streamfunction relationships are essentially of the same type.

3.3 Simulated evolution

To illustrate and validate our results for the linear dynamics, we carry out numerical simulations. Equations (2.12)–(2.13) are used to invert the potential vorticity $\hat{q}(k, l, z, t)$, for a fixed wavevector (k, l), and standard schemes (Heun method or fourth-order Runge-Kutta method) are used to advance the linear part of the prognostic equation (2.14). The resulting code serves in section 4.2 to validate by direct simulation the analytical formulas for corrections to the edge-wave frequencies. At this point, we simply illustrate the evolution of an edge wave and of perturbations from the continuous spectrum.

Figure 1 displays the evolution of an edge wave and of a perturbation in the continuous spectrum. The basic flow is chosen to describe a realistic tropopause: we introduce stratification profiles of the form

$$ S_t(Z, \, S_-, \, \Delta S, \, \alpha) = S_- + \frac{\Delta S}{2} \left(1 + \tanh \left(\frac{Z}{\alpha} \right) \right) \, , \tag{3.14} $$

where the notation

$$ \Delta S = S_+ - S_- $$

has been introduced (note that $\Delta S < 0$). For the present application, we choose $S_- = 1$, $S_+ = 1/4.5$, $\epsilon = 0.1$ and $\alpha = 1$, and the shear varies as

$$ \Sigma(z) = \begin{cases} \Sigma_- & \text{for } z < 0 \, , \\ \Sigma_+ + (\Sigma_- - \Sigma_+) \left(\cosh \left(z/\delta \right) \right)^2 \, , & \text{for } z > 0 \, . \end{cases} \tag{3.15} $$

where Σ_+ is the shear in the stratosphere, and δ is the thickness of the transition region in the shear, which is less sharp than the stratification (Birner et al. 1992). Below we will use $\delta = 3\epsilon$, as in Tomikawa et al. (2006).

The initial PV profiles, to leading order, are taken as

$$ \hat{q}_0 = \sigma' \quad \text{and} \quad \hat{q}_0 = z e^{-z^2/\epsilon^2} \, , $$

so as to satisfy (3.2) and (3.3), corresponding to an edge wave and to a perturbation in the continuous spectrum, respectively. Order-one corrections, calculated as described in sections 3.1 and 3.2, are added to these profiles in order that the separation between egde wave and continuous spectrum be accurate to $O(\epsilon)$. For both simulations the wavevector is chosen as $(k, l) = (1, 0)$.

The edge-wave solution (left panels) preserves its structure, whereas the continous-spectrum perturbation (right panels) is sheared away to smaller and smaller scales, as expected. If the order-one corrections are not included (not shown), the evolution of both initial conditions becomes
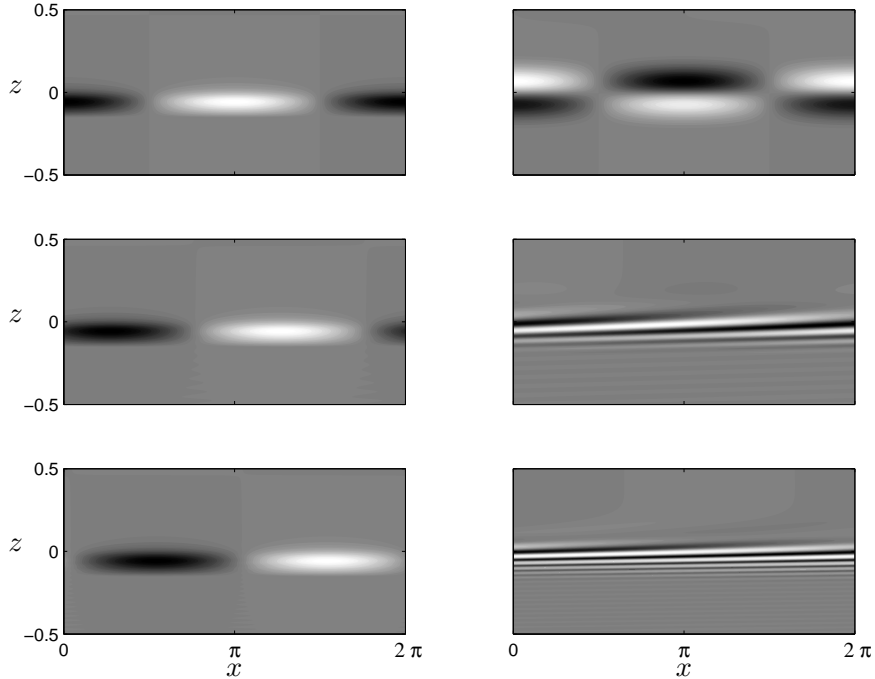
10

Figure 1: *Evolution of the perturbation PV q for monochromatic perturbations (k = 1, l = 0) in the vertical (x, z)-plane, at times t = 0, 115 and 230. Initial conditions are for an edge wave $\hat{q} = \sigma' + O(\epsilon)$ (left panels), and for a perturbation in the continuous spectrum $\hat{q} = ze^{-z^2/(2\epsilon)} + O(\epsilon)$ (right panels). For both cases, the $O(\epsilon)$ terms in the initial conditions are calculated as described in sections 3.1 and 3.2 respectively.*

'mixed': the first includes a weak component that is sheared to smaller scales, whereas the second slowly yields a weak edge wave signal emerging above the sheared disturbance. The reason is, as noted earlier, that the conditions (3.2) and (3.3) differentiate between edge wave and continuous spectrum to leading order only. The simulations confirm the relevance of the corrections calculated above.

The evolution of the energy is shown in Figure 2, confirming the conservation of energy for the edge wave solution. After an initial adjustment, the sheared disturbance of the continuous spectrum is found to decay asymptotically as t^{-2}, as predicted.

4   Correction to the SQG edge wave

We now examine the impact of the finite depth of the tropopause on edge waves. We focus mostly on the first-order, $O(\epsilon)$, correction to their frequency (sections 4.2 and 4.3), but also present the corresponding corrections to the vertical structure (section 4.4). The correction to the frequency (3.7) can be split into two contributions,

$$\omega_{1a} = \frac{-k}{\sigma_+ - \sigma_-} \int_{-\infty}^{\infty} \sigma'(Z)\hat{\psi}_0^{(1)}\,\mathrm{d}Z \quad \text{and} \quad \omega_{1b} = \frac{k}{\sigma_+ - \sigma_-} \int_{-\infty}^{\infty} \sigma'(Z)\upsilon(Z)\,\mathrm{d}Z. \tag{4.1}$$
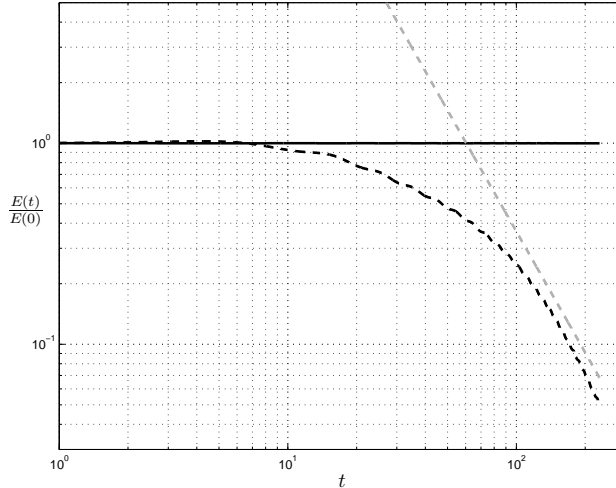
11

Figure 2: *Log-log plot of the energy of the perturbations in Figure 1 as a function of time. The energy of the edge wave (plain, black line) and of the continuous-spectrum perturbation (dashed, black line) are displayed. A gray, dashed line indicates the -2 slope corresponding to a decay of energy as t^{-2}.*

where ω_{1a} results from the first-order correction to the streamfunction, $\hat{\psi}_0^{(1)}$, while ω_{1b} only involves the profiles of the basic state in the tropopause region. In order to obtain insights regarding the different effects influencing these corrections, we consider below a number idealised profiles. As a preliminary step it is necessary to choose a definition of the tropopause that is adapted to the present discussion.

4.1 Definition of the tropopause reference level

A unique definition of the altitude of the tropopause is important in order to compare the edge-wave frequencies for different stratification profiles: since we choose to take $z = 0$ at this altitude and use a reference frame such that $U(0) = 0$, different choices for the altitude of the tropopause lead to apparently different frequencies for the same stratification profile as a result of a Doppler shift. We introduce of definition of the tropopause altitude which eliminates this ambiguity, and is adapted to the present discussion since it separates, in a relevant manner, the effect of the correction to the streamfunction, ω_{1a}, and those of the profiles of shear and stratification, ω_{1b}.

Since we use the vertical profile of $S(z)$ throughout our analysis, we decompose

$$S(z) = S_- + \Delta S\, H(z - z_t) + R(z),$$

where $H(z)$ is the Heaviside function, z_t the altitude of the tropopause, $R(z)$ is a residual. In such a decomposition, it is natural to impose that

$$\int_{-\infty}^{+\infty} R(z)\, dz = 0.$$

This constraint determines z_t, and serves as our definition for the altitude of the tropopause. Note that this definition can differ from standard definitions or intuitions. It is relevant for the present
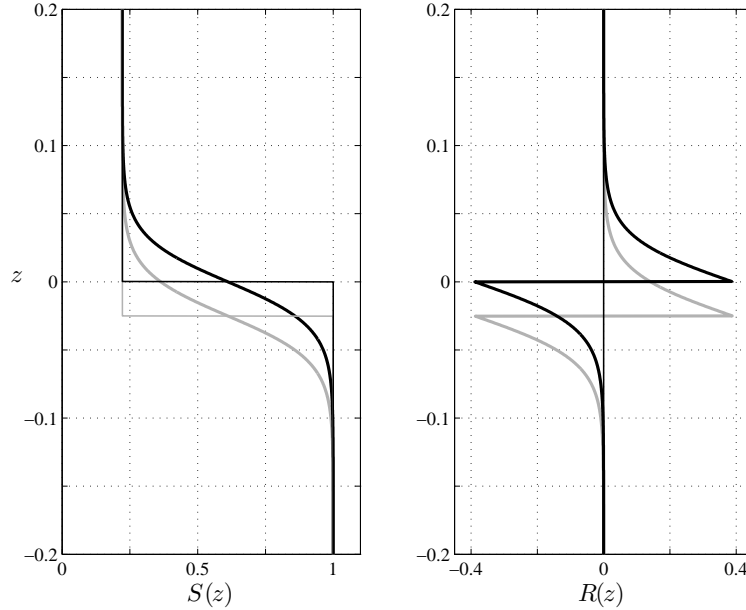
Figure 3: *(Right): Profiles of $S(z)$ (bold lines), and of their approximations $S_- + \Delta S\, H(z - z_t)$ (thin lines) for cases with a $\tanh(z/\epsilon)$ variation for S (black lines) or for N^2 (gray lines). (Left): the residuals $R(z)$ between the profiles and their approximations.*

discussion and is not meant as a novel practical definition the tropopause. As an example, Figure 3 illustrates this decomposition for two stratification profiles with a smooth $\tanh(z/\epsilon)$ transition. In the first profile, given in (3.14), $\tanh(z/\epsilon)$ is the form of $S(Z)$, whereas in the second profile it is the form of $N^2(Z) = f^2/S(Z)$. In the second case, our definition leads to a tropopause slightly below $z = 0$.

The comparison of ω_1 for different stratification profiles is meaningful only if the profiles are first shifted so as to have their tropopause at the same reference level, otherwise the comparison would be obscured by the Doppler shifts due to different reference levels. In what follows we describe flows with the height coordinate changed in order to have $z_t = 0$ and in a frame of reference such that $U(0) = 0$.

4.2 Constant shear

First, we consider the simple case of a constant shear, $\Sigma = $ const, when ω_1 reduces to (3.9). To begin with the simplest stratification profile, the case of a piecewise linear S is considered:

$$S(Z) = \begin{cases} S_+ & \text{for } \epsilon < z, \\ (S_+ + S_-)/2 + Z\,(S_+ - S_-)/2 & \text{for } -\epsilon < z < \epsilon, \\ S_- & \text{for } z < -\epsilon. \end{cases} \qquad (4.2)$$

13

For this configuration, ω_1 is explicitly calculated from (3.9) as

$$\omega_1 = -\Sigma\,k\frac{2}{\Delta S}\left(\left(\frac{S_- + S_+}{2}\right) + \frac{S_+\,S_-}{\Delta S}\log\frac{S_-}{S_+}\right) . \qquad (4.3)$$

Although it may appear that there are two parameters, S_+ and S_-, defining the basic stratification, this is misleading. It is possible to rewrite the correction (4.3) in terms of the relative jump in stratification $\Delta s = \Delta S/S_-$ as

$$\omega_1 = -\Sigma\,k\frac{2}{\Delta s}\left(1 + \frac{\Delta s}{2} - (1 + \Delta s)\frac{\log(1 + \Delta s)}{\Delta s}\right) . \qquad (4.4)$$

This expression has the advantage of making it easier to see that, for small stratification jumps $|\Delta s| \ll 1$, ω_1 becomes proportional to Δs: expanding the logarithm yields

$$\omega_1 = -\Sigma\,k\,\frac{\Delta s}{3} + O\left((\Delta s)^2\right) . \qquad (4.5)$$

More generally, Δs varies between 0 (hardly any PV jump across the tropopause) to -1 (infinite stratification above the tropopause, i.e. the tropopause is a rigid lid). For the simple stratification given by (4.2), the variations of ω_1 with Δs are illustrated in figure 4. This correction is always positive, corresponding to a slowing down of the westward phase speed of the edge waves.

To illustrate the sensitivity of the correction to the precise shape of the stratification across the tropopause, figure 4 also includes ω_1 predicted for a stratification given by $S_t(Z, 1, \Delta s, 2/3)$, with S_t is defined in (3.14). The value $\alpha = 2/3$ was chosen so that the corrections are identical for small $|\Delta s|$. It is found that, for reasonable values of Δs, say $\Delta s > -0.80$, the correction is not sensitive to the fine details of $S(Z)$. Hence, the analytical formula (4.4) can be taken as a good estimate of ω_1 for such smooth transitions. The correction ω_1 does become sensitive to the details of $S(Z)$ for very strong stratification jumps, i.e. $\Delta s < -0.90$.

Finally, we test the result (4.4) using the numerical code described in section 3.3 to determine numerically the frequency of edge waves. The order-one correction to the structure of the edge wave, as described in section 3.1, is included, and a resolution of 200 points in the vertical is found to be sufficient. Excellent agreement is found, as shown in Fig. 4, providing a further validation for the code and the analytical results.

Although profiles (4.2) or (3.14) are natural candidates for a simple finite-depth version of a discontinuous stratification profile, observations may motivate a different choice for the typical transition at the tropopause: in a study of 10 years of twice-daily high-resolution radiosonde profiles from two stations in southern Germany, Birner, Dörnbrack & Schumann (1992) analyzed the static stability in the vicinity of the tropopause. They produced a climatology by composing a large number of profiles with the thermal tropopause as a common reference level, and showed that in individual profiles the tropopause occurs as a very sharp transition in the Brunt-Väisälä frequency, with a maximum just above this sharp transition. The effect of such a feature on the frequency of edge-waves is now investigated.
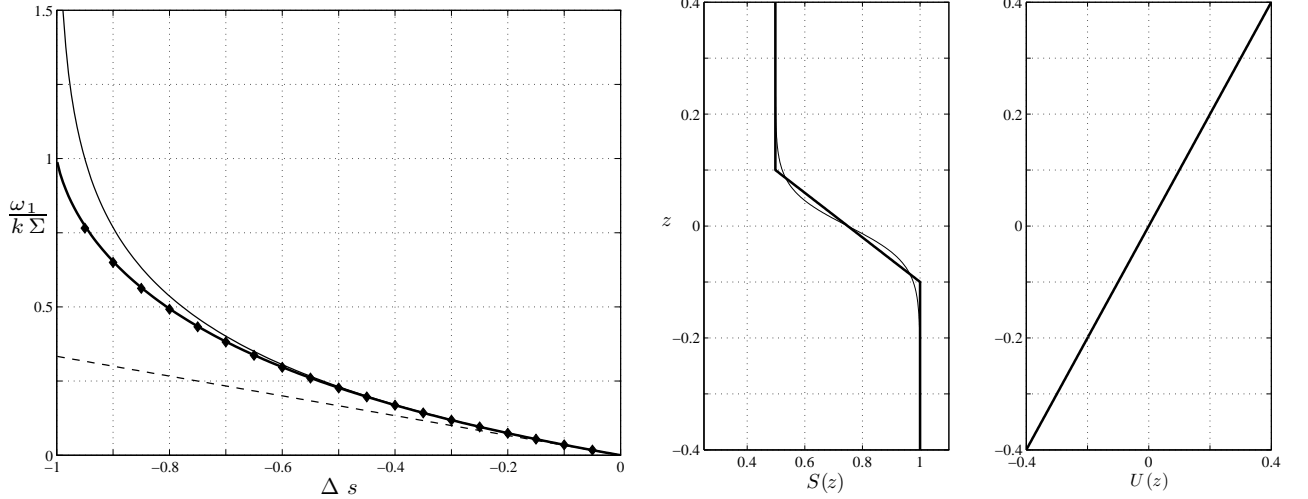
Figure 4: *(Left) First-order correction ω_1 to the edge-wave frequency as a function of the relative stratification jump across the tropopause Δs for the case of a constant shear and piecewise linear $S(Z)$ given in (4.2). Vertical profiles of $S(z)$ (middle) and $U(z)$ (right), for the specific choice of parameters $\epsilon = 1$, $\Sigma = 1$, $S_- = 1$ and $S_+ = 0.5$. Two profiles of $S(z)$ are shown: piecewise linear (black solid line, equation (4.2)), and hyperbolic tangent (gray solid line, equation (3.14) with $\alpha = 2/3$). Also shown are: the linear approximation (4.5) for ω_1 (dashed line), and estimates of ω_1 obtained in numerical simulations of the linear dynamics with the piecewise linear profile of $S(Z)$ (symbols).*

Four basic profiles for the stratification are considered:

$$S_1(z) = S_t(\epsilon^{-1} z, \, 1, \, \Delta s, \, 2/3), \tag{4.6}$$

$$S_2(z) = S_t(\epsilon^{-1} (z - z_t), \, 1, \, \Delta s, \, 2/3) + B(z - z_t),$$

$$S_3(z) = S_t(\epsilon^{-1} (z - z_t), \, 1, \, \Delta s, \, 1/3) + B(z - z_t), \tag{4.7}$$

$$S_4(z) = S_- + \Delta S H(z - z_t) + B(z - z_t), \tag{4.8}$$

$$\text{where} \quad B(z) = \Delta s \, \frac{1 + \Delta s}{1 - \Delta s} \, e^{-z/\epsilon} \, H(z),$$

with S_t defined in (3.14). The form of $B(z)$ is chosen such that, in S_4, the jump of N^2 across $z = 0$ be twice the difference $N_+^2 - N_-^2$. The other two profiles S_2 and S_3 are intermediate between S_1 and S_4. Note that the profiles now include a discontinuity and that S_4 is monotonically increasing, not decreasing, above the tropopause. The profiles are shifted vertically as described in section 4.1, hence the presence of z_t in (4.6).

The corresponding corrections ω_1 are shown in Figure 5. Examination of ω_1 for the stratification profile $S_4(z)$ (thick curve in Figure 5) shows that the effect of the enhanced stratification right above the tropopause is to decrease the frequency of the edge wave (negative ω_1, or stronger westward phase speed). This is a fraction of the decrease that would be obtained if the stratification of the stratosphere is increased overall, i.e. if S_+ was lowered. The intensity of this correction of course increases with the depth over which the stratification is enhanced. For profiles $S_2(z)$ and
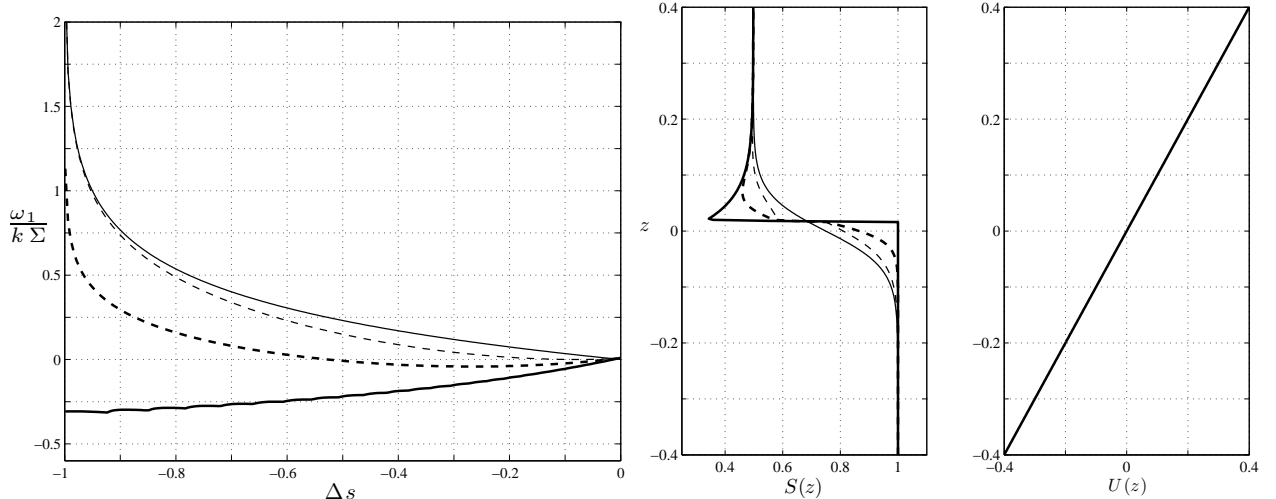
15

Figure 5: *Same as Figure 4 but for a stratification including a peak in stratification above the tropopause, as defined in (4.6): S_1 (thin line), S_2 (thin, dashed line), S_3 (thick, dashed line) and S_4 (thick line).*

$S_3(z)$ which are intermediate, the effect of the smooth transition and of the enhanced stratospheric stratification compensate each other to a large extent, leading to weak corrections for realistic values of Δs.

In practice it is not clear which is the most relevant choice for the tropopause, i.e. whether the edge waves will be sensitive to this local maximum in stratification of whether this peak will be averaged out in a description of the tropopause on the typical scale of edge waves. The above results suggest that if both aspects contribute (finite depth and enhanced stratification right above the tropopause) their effects may cancel out to some degree, making the SQG prediction for the edge-wave frequency a better approximation than could be expected.

4.3 Variable shear

The effect of a profile with variable shear is now investigated. Profiles similar to those of Tomikawa et al. (2006) (cf. their Appendix A) are used: $S = S_t(Z, 1, \Delta s, 2/3)$ and $\Sigma(z)$ given as in (3.15).

Differences in the stratospheric shear modify the frequency of the edge waves both at order 0 and 1. Hence, Figure 6 shows the frequencies ω_0 (gray lines) and $\omega_0 + \epsilon\omega_1$ (black lines) as a function of Δs, for four values of the stratospheric shear: $\Sigma_+ = 1$, for reference, and $\Sigma_+ = 0.5$, 0 and -0.5.

As $\Delta s \to 0$, the PV jump at the tropopause becomes due essentially to the discrepancy between Σ_- and Σ_+. For the curves with $\Sigma_+ \neq \Sigma_-$, this sets a finite value for ω_0. In contrast, as $\Delta s \to -1$, the PV jump at the tropopause is dominated by the stratification, and all curves converge, regardless of Σ_+.

The corrections ω_1 are always positive. Indeed, the smooth transition at the tropopause leads to stronger winds in the lower stratosphere than for a discontinuous profile. Consistently, the corrections are found to increase with δ (not shown) and to increase as Σ_+ decreases. In consequence, for realistic values of Δs, the range of corrected frequencies $\omega_0 + \epsilon\omega_1$ is narrower than that of ω_0,
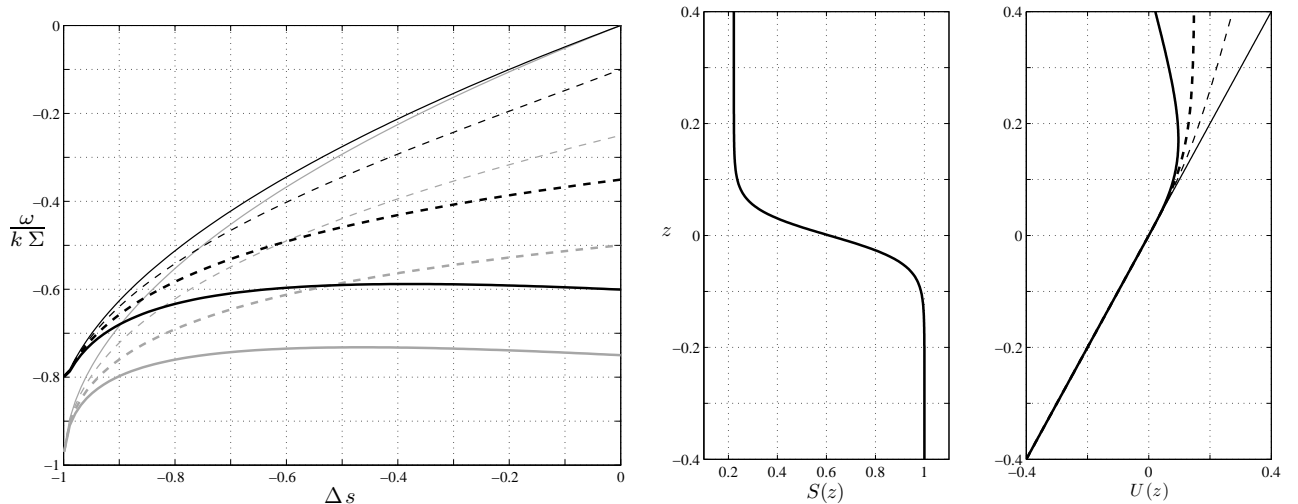
16

Figure 6: *Same as Figure 4 but for* ω_0 *(gray lines) and* $\omega_0 + \epsilon\omega_1$ *(black lines), with* $S(z)$ *and* $\Sigma(z)$ *as defined in (3.15). Four different values are used for* Σ_+: *1 (thin line), 0.5 (thin, dashed), 0 (thick, dashed) and -0.5 (thick).*

e.g. for $\Delta s = -0.8$, these ranges are respectively of 0.11 and 0.20. Therefore, SQG estimates of edge-wave frequencies overestimate the impact of the difference between tropospheric and stratospheric shear. This is all the more true as δ/ϵ is large, i.e. as the transition at the tropopause is sharper in the stratification than in the shear, as is the case in observations (Birner et al. 1992).

4.4 Spatial correction and energy

Our model for the dynamics of disturbances to a finite-decpth tropopause also provides the order-one corrections to the vertical structure of the edge-waves. Such corrections have been the subject of previous investigations (Rivest & Farrell 1992, Muraki & Hakim 2001), and have been helped to explain the distribution of kinetic and potential energy in edge waves found in analyses (Tomikawa et al. 2006). Indeed, two observed features differed remarkably from the distribution expected from SQG: the potential energy (PE) goes through a minimum near the tropopause, while kinetic energy (KE) there is maximum. This yields a minimum in the ratio PE/KE, whereas SQG predicts that this ratio should be equal to 1 everywhere. The second feature is that KE in the stratosphere is stronger than PE, yielding a ratio PE/KE significantly smaller than 1 above the tropopause. We now show how our model straightforwardly explains the first feature, while the second is outside its scope.

By construction, our solution contrasts with the SQG edgewave by the fact that it has a continuous derivative at the tropopause, as illustrated in Figure 7. With PE and KE are defined as:

$$\text{PE} = \frac{1}{2} \iint S \left(\partial_z \psi \right)^2 \mathrm{d}x\,\mathrm{d}y \;, \quad \text{KE} = \frac{1}{2} \iint \left(\nabla_H \psi \right)^2 \mathrm{d}x\,\mathrm{d}y \;,$$

the continuity of $\partial_z \psi$, and the fact that ψ increases in the troposphere and decreases in the stratosphere immediately implies, that there is a height near the tropopause where $\partial_z \psi(z) = 0$, yielding $PE(z) = 0$. Hence, the minimum in PE and in PE/KE observed at the tropopause is a direct
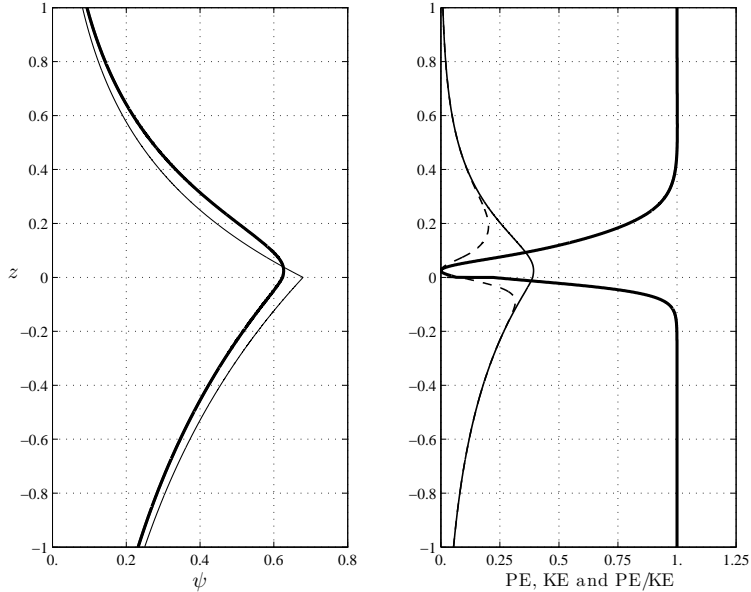
Figure 7: *(Right): The streamfunction according to SQG (thin line) and to our model (up to order 1, thick line) for an edge wave with $k = 1$, $l = 0$, with the stratification and shear chosen as in section 3.3. (Left): Potential energy (thin, dashed line), kinetic energy (thin line) and ratio PE/KE (thick line) for our solution.*

consequence of the finite-depth of the tropopause and the continuity of ψ and S there, as illustrated in Figure 7. This was shown by Tomikawa et al. (2006), who calculated numerically the eigenfunctions for a specific stratification and shear, following Rivest & Farrell (1992). Our model makes it straightforward to calculate the distributions of PE and KE, and describe precisely the minimum in PE near the tropopause (Figure 7).

Regarding the second feature highlighted in the observations by Tomikawa et al. (2006), i.e. the weaker PE/KE in the stratosphere, our model does not provide any insights: indeed, the structure of the streamfunction outside the tropopause region (see (2.4)) is the same as in the SQG model, yielding a ratio PE/KE = 1.

5   Discussion

In this paper, we use matched asymptotics to derive a simplified model for the quasi-geostrophic evolution of perturbations localised near the tropopause. This takes advantage of the separation between the vertical scale of typical perturbations (estimated as f/N times their horizontal scales), and the depth of the tropopause. To leading order, the SQG model of Juckes (1994) is recovered. In this two-dimensional model, the depth-integrated PV of the perturbations, which can be interpreted as a potential temperature, controls the dynamics; the only backround property that matters is the PV jump across the tropopause. The model obtained at the next order, on which we focus, remains three-dimensional and depends explicitly on the shear and stratification profiles of the tropopause. This model consists of the prognostic equation (2.14) for the PV perturbation together

with the inversion relations (2.12)–(2.13). Compared to the parent quasi-geostrophic model, the main simplifications are (i) the focus on the tropopause region, which relies on analytic solutions for the flow outside; and (ii) the one-dimensional, columnar inversion relation, which results from the anisotropy of the flow. Compared with SQG, a crucial ingredient that is added is the vertical shearing of the perturbation PV by the background horizontal wind. Because of this, and because of the vertical dependence of the perturbation streamfunction, the vertically-integrated PV is not materially conserved as it is in SQG.

In the linear regime, the model describes two types of modes. The first type of modes are the westward-propagating edge waves. For these, the model provides corrections to the frequency and vertical structure found in SQG. The second type of modes correspond to a continuous spectrum of singular modes which represent disturbances whose PV is sheared to ever finer scales by the background flow. The corresponding streamfunction and energy decrease like t^{-2}. These modes have zero vertically-integrated PV (to leading order), and they are completely filtered out by the SQG approximation. Our results for the vertical structure of the edge waves ((3.2)–(3.11)) and of the continuous spectrum ((3.3)–(3.13)) make it possible to separate arbitrary initial conditions into edge-wave and continuous-spectrum components. Specifically, for each horizontal wavevector (k, l), one can find a (complex) scalar defining the amplitude of the edge wave with this wavevector, and a (complex) function of Z with zero integral defining the continuous-spectrum contribution to the PV. These scalar and function can be computed order-by-order in ϵ, starting with the separation of the initial PV into vertically-integrated and zero-mean parts.

The sensitivity of the edge-wave frequency to the details of the shear and stratification profiles in the tropopause region is examined in this paper by considering simple model profiles. The leading-order frequency (3.1) found in the SQG approximation is corrected at $O(\epsilon)$ as a result of the vertical shear and of the Z-dependence of the streamfunction. Evaluating this correction shows that the SQG approximation overestimates (in absolute value) the frequency of the edge waves, with smoother stratification profiles leading to lower frequencies than sharp ones. This effect is reduced, however, if the stratification profile takes into account the overshoot in N that has been observed just above the tropopause (Birner et al. 1992). Smoothness in the shear also decreases (in absolute value) the frequency of the edge waves, mainly because the PV jump associated with the change between tropospheric and stratospheric shears is effectively reduced. Spatial corrections to the vertical structure of the edge wave are also obtained: the presence of a minimum in the potential energy, near the tropopause, is a consequence of the finite-depth of the tropopause (Tomikawa et al. 2006), and the precise structure of this minimum can be calculated for arbitrary stratification and shear profiles using our model.

Although we focus our attention on the linear regime, the asymptotic model derived in this paper is nonlinear and could be exploited to study a range of phenomena. Of particular interest, perhaps, is the nonlinear interaction between the edge waves and the continuous spectrum, since the latter is completely neglected in the SQG approximation. It should be noted, however, that the assumption of anisotropic disturbances which underlies our model may not be consistent over long time scales, in particular if instabilities with small horizontal scales develop (cf. Haynes 1987).

A   Derivation of (2.12)–(2.13)

Consider (2.10) first. It is convenient to use the Fourier transforms of the dependent variables and ignore their dependencies in (k, l, t) for the moment. Defining

$$\hat{P}(Z) = \int_0^Z \hat{q}(Z') \, \mathrm{d}Z', \tag{A.1}$$

we integrate (2.10) once as

$$S\partial_Z \hat{\psi}^{(1)} = \hat{P}(Z) + C_1, \tag{A.2}$$

where C_1 is a 'constant' (i.e. independent of Z). Dividing by S and integrating once more then gives

$$\hat{\psi}^{(1)} = \int_0^Z \frac{\hat{P}(Z') + C_1}{S(Z')} \, \mathrm{d}Z' + C_2. \tag{A.3}$$

Expressions relating $\hat{\psi}^{(0)}$, C_1 and C_2 to $\hat{q}$ are found from the matching conditions. We first note the asymptotics

$$\hat{\psi}^{(1)} = \frac{\hat{P}_\pm + C_1}{S_\pm} Z + \int_0^{\pm\infty} \left(\frac{\hat{P}(Z') + C_1}{S(Z')} - \frac{\hat{P}_\pm + C_1}{S_\pm} \right) \mathrm{d}Z' + C_2 + o(1). \tag{A.4}$$

as $Z \to \pm\infty$. Identifying the coefficient of Z with that of (2.8) then gives

$$\mp S_\pm^{1/2} \kappa \hat{\phi}^{(0)} = \hat{P}_\pm + C_1 \tag{A.5}$$

It follows that

$$-(S_+^{1/2} + S_-^{1/2}) \kappa \hat{\phi}^{(0)} = \hat{P}_+ - \hat{P}_- = \int_{-\infty}^\infty \hat{q}(Z) \, \mathrm{d}Z. \tag{A.6}$$

Since $\hat{\psi}^{(0)} = \hat{\phi}^{(0)}$, this equation determines $\psi^{(0)}$ in terms of q as given in (2.12). It also follows from (A.5) that

$$C_1 = -\frac{S_-^{1/2}}{S_+^{1/2} + S_-^{1/2}} \hat{P}_+ - \frac{S_+^{1/2}}{S_+^{1/2} + S_-^{1/2}} \hat{P}_-. \tag{A.7}$$

Identifying the Z-independent terms in (2.8) and (A.4) gives

$$\hat{\phi}_\pm^{(1)} = \int_0^{\pm\infty} \left(\frac{\hat{P}(Z') + C_1}{S(Z')} - \frac{\hat{P}_\pm + C_1}{S_\pm} \right) \mathrm{d}Z' + C_2. \tag{A.8}$$

Another equation is needed to determine C_2 and hence $\hat{\psi}^{(1)}$. This is derived by integrating (2.11) once, computing

$$\left[S\partial_Z \hat{\psi}_2 - \kappa^2 Z \hat{\psi}^{(0)} \right]_{-\infty}^\infty = 0,$$

and using (2.9) to obtain

$$S_+^{1/2} \hat{\phi}_+^{(1)} + S_-^{1/2} \hat{\phi}_-^{(1)} = 0.$$

Combining with (A.8) gives

$$C_2 = \frac{-1}{S_+^{1/2} + S_-^{1/2}} \left[S_+^{1/2} \int_0^\infty \left(\frac{\hat{P}(Z') + C_1}{S(Z')} - \frac{\hat{P}_+ + C_1}{S_+} \right) dZ' \right.$$

$$\left. + S_-^{1/2} \int_0^{-\infty} \left(\frac{\hat{P}(Z') + C_1}{S(Z')} - \frac{\hat{P}_- + C_1}{S_-} \right) dZ' \right]. \qquad (A.9)$$

With C_1 and C_2 determined by (A.7) and (A.9), $\hat{\psi}^{(1)}$ in (A.3) is now fully determined. To obtain a simple, explicit expression for $\hat{\psi}^{(1)}$, we start by writing

$$\hat{\psi}^{(1)} = -\frac{S_+^{1/2}}{S_+^{1/2} + S_-^{1/2}} \int_Z^\infty \left(\frac{\hat{P}(Z') + C_1}{S(Z')} - \frac{\hat{P}_+ + C_1}{S_+} \right) dZ' + \frac{\hat{P}_+ + C_1}{S_+^{1/2}(S_+^{1/2} + S_-^{1/2})} Z$$

$$+ \frac{S_-^{1/2}}{S_+^{1/2} + S_-^{1/2}} \int_{-\infty}^Z \left(\frac{\hat{P}(Z') + C_1}{S(Z')} - \frac{\hat{P}_- + C_1}{S_-} \right) dZ' + \frac{\hat{P}_- + C_1}{S_-^{1/2}(S_+^{1/2} + S_-^{1/2})} Z. \quad (A.10)$$

Now, we note from (A.1) and (A.7) that

$$\hat{P} + C_1 = -\frac{S_-^{1/2}}{S_+^{1/2} + S_-^{1/2}} \int_Z^\infty \hat{q}(Z') \, dZ' + \frac{S_+^{1/2}}{S_+^{1/2} + S_-^{1/2}} \int_{-\infty}^Z \hat{q}(Z') \, dZ',$$

and hence that

$$\hat{P}_+ + C_1 = \frac{S_+^{1/2}}{S_+^{1/2} + S_-^{1/2}} \hat{\theta} \quad \text{and} \quad \hat{P}_- + C_1 = -\frac{S_-^{1/2}}{S_+^{1/2} + S_-^{1/2}} \hat{\theta}.$$

Introducing these expressions into (A.10), using the definition (A.1) of $\hat{P}$, and the expansions

$$\frac{\hat{P} + C_1}{S} - \frac{\hat{P}_\pm + C_1}{S_\pm} = \left(\frac{\hat{P} + C_1}{S} - \frac{\hat{P}_\pm + C_1}{S} \right) + \left(\frac{\hat{P}_\pm + C_1}{S} - \frac{\hat{P}_\pm + C_1}{S_\pm} \right)$$

then leads to (2.13).

B Derivation of (3.8)

Introducing $\hat{q} = \hat{q}_0 = \sigma'$ into (2.13) gives

$$\hat{\psi}_0^{(1)} = \int_Z^\infty \frac{(S_+ S_-)^{1/2}[\sigma_+ - \sigma(Z')] + \sigma_-[S_+ - S(Z')] + \sigma_+ S(Z') - \sigma(Z')S_+}{\left(S_+^{1/2} + S_-^{1/2} \right)^2 S(Z')} dZ'$$

$$+ \int_{-\infty}^Z \frac{(S_+ S_-)^{1/2}[\sigma(Z') - \sigma_-] + \sigma_+[S(Z') - S_-] + \sigma(Z')S_- - \sigma_- S(Z')}{\left(S_+^{1/2} + S_-^{1/2} \right)^2 S(Z')} dZ',$$

after some simplification. Introducing this expression into the first term of (3.7) and integrating by parts gives

$$\int_{-\infty}^{\infty} \sigma'(Z)\hat{\psi}_0^{(1)}\,\mathrm{d}Z =$$

$$\int_{-\infty}^{\infty} \frac{2(S_+S_-)^{1/2}[\sigma^+ - \sigma(Z)][\sigma(Z) - \sigma_+] + S(Z)(\sigma_+ - \sigma_-)^2 - S_-[\sigma_+ - \sigma(Z)]^2 - S_+[\sigma(Z) - \sigma_-]^2}{\left(S_+^{1/2} + S_-^{1/2}\right)^2 S(Z)}\,\mathrm{d}Z,$$

which can be further simplified into (3.8).

References

Balmforth, N., del-Castillo-Negrete, D. & Young, W. R. (1997), 'Dynamics of vorticity defects in shear', *J. Fluid Mech.* **333**, 197–230.

Balmforth, N., Llewellyn Smith, S. G. & Young, W. R. (2001), 'Disturbing vortices', *J. Fluid Mech.* **426**, 95–133.

Birner, T., Dörnbrack, A. & Schumann, U. (1992), 'How sharp is the tropopause at midlatitudes?', *Geophys. Res. Lett.* **29**, 1700.

Blumen, W. (1978), 'Uniform potential vorticity flow. Part I: theory of wave interactions and two-dimensional turbulence', *J. Atmos. Sci.* **35**, 421–432.

Briggs, R. J., Daugherty, J. D. & Levy, R. H. (1970), 'Role of Landau damping in crossed-field electron beams and inviscid shear flows', *Phys. Fluids* **13**, 421–432.

Hakim, G. J., Snyder, C. & Muraki, D. J. (2002), 'A new surface model for cyclone-anticyclone asymmetry', *J. Atmos. Sci.* **59**, 2405–2420.

Haynes, P. H. (1987), 'On the instability of sheared disturbances', *J. Fluid Mech.* **175**, 463–478.

Held, I., Pierrehumbert, R., Garner, S. & Swanson, K. (1995), 'Surface quasi-geostrophic dynamics', *J. Fluid Mech.* **282**, 1–20.

Hoskins, B. J., McIntyre, M. & Robertson, A. (1985), 'On the use and significance of isentropic potential vorticity maps', *Quart. J. R. Met. Soc.* **111**, 877–946.

Juckes, M. (1994), 'Quasi-geostrophic dynamics of the tropopause', *J. Atmos. Sci.* **51**, 2756–2768.

Kiselev, A., Nazarov, F. & Volberg, A. (2007), 'Global well-posedness for the critical 2D dissipative quasi-geostrophic equation', *Invent. Math.* **167**, 445–453.

Lapeyre, G. & Klein, P. (2006), 'Dynamics of the upper oceanic layers in terms of surface quasi-geostrophy theory', *J. Phys. Oceanogr.* **36**, 165–176.

Muraki, D. & Hakim, G. J. (2001), 'Balanced asymmetries of waves on the tropopause', *J. Atmos. Sci.* **58**, 237–252.

Pierrehumbert, R. T., Held, I. M. & Swanson, K. L. (1994), 'Spectra of local and non-local two-dimensional turbulence', *Chaos, Solitons & Fractals* **4**, 1111–1116.

Rivest, C., Davis, C. A. & Farrell, B. F. (1992), 'Upper-tropospheric synoptic-scale waves. Part I: Maintenance as Eady normal modes', *J. Atmos. Sci.* **49**, 2108–1219.

Rivest, C. & Farrell, B. F. (1992), 'Upper-tropospheric synoptic-scale waves. Part II: Maintenance and excitation of quasi-modes', *J. Atmos. Sci.* **49**, 2120–2138.

Samelson, R. M. (1999), 'Note on a baroclinic analogue of vorticity defects in shear', *J. Fluid Mech.* **382**, 367–373.

Stewartson, K. (1981), 'Marginally stable inviscid flows with critical layers', *I.M.A. J. Appl. Math.* **27**, 133–175.

Tomikawa, Y., Sato, K. & Shepherd, T. G. (2006), 'A diagnostic study of waves on the tropopause', *J. Atmos. Sci.* **63**, 3315–3316.

Tulloch, R. & Smith, K. S. (2006), 'A theory for the atmospheric energy spectrum: Depth-limited temperature anomalies at the tropopause', *Proc. Nat. Acad. Sci.* **103**, 14690–14694.